Materials Research Proceedings **32** (2023) 362-370 https://doi.org/10.21741/9781644902615-41

Texture and strain rate sensitivity analysis of solid solution and precipitation hardening aluminum alloys processed by repetitive corrugation and straightening

Sergio Elizalde[1,2,a], Marco Ezequiel[1,3,b], Liliana Romero-Resendiz[1,4,c], Jose Maria Cabrera[2,5,d], Gonzalo González[1,e*]

[1] Instituto de Investigaciones en Materiales, Universidad Nacional Autónoma de México, Circuito Exterior S/N, Cd. Universitaria, A. P. 70-360, Coyoacán, C.P. 04510, Mexico.

[2] Departamento de Ciencia e Ingeniería de Materiales, EEBE - Universidad Politécnica de Cataluña, c/Eduard Maristany 10-14, 08019 Barcelona, Spain

[3] Univ. Lille, CNRS, INRAE, Centrale Lille, UMR 8207 - UMET - Unité Matériaux et Transformations, F-59000 Lille, France

[4] Facultad de Química, Departamento de Ingeniería Metalúrgica, Universidad Nacional Autónoma de México, México City, 04510, Mexico

[5] Fundación CIM UPC, c/Llorens i Artigas 12, 08028 Barcelona, Spain

[a]sergio.elizalde@upc.edu, [b]ezequielam@univ-lille.fr, [c]liliana.rom7@comunidad.unam.mx, [d]jose.maria.cabrera@upc.edu, [e]joseggr@unam.mx

Keywords: Aluminum Alloys; Texture; Strain-Rate Sensitivity; Repetitive Corrugation and Straightening

Abstract. The potential of improving the mechanical strength by the RCS process is evaluated on the 5754, 6061, and 7075 aluminum alloys, which present different hardening mechanisms related to their respective alloying elements. This work compares the evolution of the texture and the mechanical properties of the different alloys through the RCS processing. The mechanical properties were evaluated by micro-hardness measurements, tensile tests at different temperatures, and strain rates to evaluate the strain-rate sensitivity. The results showed that after two RCS passes, the 6061 and 5754 alloys showed a relatively high strain-rate sensitivity at 300°C. In addition, an increment of 27%, 22%, 15% in hardness was obtained for the 5754, 6061 and 7075 alloys, respectively. Showing the potential of improvement in the mechanical resistance due to the different hardening mechanism. Furthermore, the crystallographic texture was characterized by the obtention of pole figures by X-ray diffraction and the calculation of their orientation distribution functions. The results showed the same trend in the three aluminum alloys, i.e., the initial texture components were conserved, but the texturized volume decreased.

Introduction

Aluminum alloys have excellent mechanical properties, low density, corrosion resistance, and recyclability, making them promising alternatives to some steel components in the automotive industry. Despite these advantages, their lower formability and significant spring back at room temperature constrain the application of aluminum alloys [1,2]. To overcome these disadvantages, recent studies have focused on reducing the grain size of these alloys to an ultrafine level to improve the mechanical properties of the alloys, as smaller grain sizes typically contribute to enhanced strength and hardness. Severe plastic deformation (SPD) techniques can significantly decrease the grain size and increase the mechanical properties; some examples are equal channel angular pressing (ECAP), high-pressure torsion (HPT), accumulative roll bonding (ARB), equal

Materials Research Proceedings **32** (2023) 362-370 https://doi.org/10.21741/9781644902615-41

channel angular rolling (ECAR), constrained groove pressing (CGP), and repetitive corrugation and straightening (RCS) [3–6].

Most SPD techniques induce repetitive plastic deformation, overcoming standard deformation limits without significantly changing the initial shape. Since many modern engineering applications require metal sheets, SPD processes on such geometries are particularly interesting. ECAR, ARB, CGP, and RCS allow deforming materials in sheet format while maintaining the dimensions and shape of the material. Particularly, ARB is a simple and continuous process, but it requires special surface treatment to prevent bonding failure. In contrast, RCS requires no special surface treatment and offers more flexibility in improving mechanical properties by modifying die geometries and deformation routes. Exploring these techniques and processes presents a promising avenue for enhancing aluminum formability and mechanical properties for industrial applications [8].

Despite the development of these techniques, the lack of knowledge regarding post-SPD shaping hinders the broader commercialization of these SPD-processed materials [9,10]. Increasing the forming temperature is one proposed solution to enhance the post-SPD shaping of aluminum alloys. In this context, the strain rate sensitivity parameter becomes an essential indicator of the forming capacity, illustrating the ability of the material to sustain homogeneous deformation and delay fracture under the applied strain rate [1]. In addition, the grain size, notably when reduced to below 10 μm, significantly affects the hot forming processes, even being capable of inducing superplastic behavior and resulting in extraordinary homogeneous elongations [11].

On the other hand, the crystalline orientation distribution within a polycrystalline material, i.e., the crystallographic texture, significantly impacts mechanical properties such as anisotropy, formability, strain hardening, and post-forming surface roughness. In that sense, the material texture influences the rate and magnitude of strain hardening during deformation. Consequently, comprehending and controlling crystallographic texture is critical for optimizing metallic materials for specific manufacturing applications [12,13].

In aluminum alloys, crystallographic texture evolution typically manifests specific orientations during different manufacturing processes. For example, the texture generally evolves around the so-called copper, brass, and S orientations during the rolling process. In contrast, the annealing process often develops the Cube and Goss orientations. The impact of these texture components on the formability of aluminum alloys is a topic of ongoing debate in the scientific community. For example, some researchers argue that the cube texture component is beneficial in enhancing formability, while others contest that it might have a detrimental effect [14,15].

Aluminum alloys 5754, 6061, and 7075 have distinct hardening mechanisms due to their unique compositions and microstructural characteristics. The 5754 alloy is a non-heat treatable alloy with medium strength. Its hardening mechanism mainly relates to solid solution strengthening and strain hardening. Solid solution strengthening occurs due to the alloying elements (such as magnesium), which distort the lattice structure when added to the aluminum matrix, creating resistance to dislocation movement. This resistance enhances the strength of the material. Strain hardening, also known as work hardening, is the process by which the material becomes stronger as it is deformed, with dislocations in the crystal structure interacting and multiplying to create a harder and stronger material [16].

On the other hand, the 6061 and 7075 alloys are heat-treatable with medium to high strength. Their hardening mechanism relies on precipitation. This process involves three stages: solution heat treatment, quenching, and aging. Solution heat treatment dissolves the soluble alloying elements within the aluminum matrix, followed by rapid quenching to retain them in a super-saturated solid solution. During aging, these elements precipitate out of the solution, forming fine particles that hinder dislocation movement, increasing the alloy's strength and hardness. Therefore, the hardening mechanism is the primary difference between the studied alloys [16].

The objective of the present work is to compare the hardening evolution and hot formability of different aluminum alloys and the effect of the RCS on the crystallographic texture evolution through the process. Furthermore, the strain rate sensitivity is evaluated by hot tensile tests to characterize the RCS impact on the hot formability. Moreover, a quantitative analysis of the texture evolution is assessed by identifying the different texture components and calculating their respective volume fraction through the orientation distribution functions.

Methods

Commercially available 5754-H111, 6061-T6, and 7075-O aluminum sheets with 1 mm thickness were cut into squares of 120 x 120 mm. Table 1 summarizes the nominal chemical composition of these alloys. A pair of dies, fabricated from D2 tool steel and featuring a geometry based on two perpendicular extruded cuts with a sinusoidal profile, were used for the corrugation stages. A pair of analogous flat dies made of D2 steel were used for the straightening stages. The modified RCS process allows the alternation of the deformed zone with each pressing, and it consists of pressing the sheets and then rotating them 90° around the normal direction to generate alternated zone with low and high deformation levels. The semi-circular profile avoids stress concentrations in comparison to a V-groove profile, and it introduces less stress concentration points [17]. Every sequence of corrugation, straightening, 90° rotation, corrugation, and straightening is considered one RCS pass (Fig. 1).

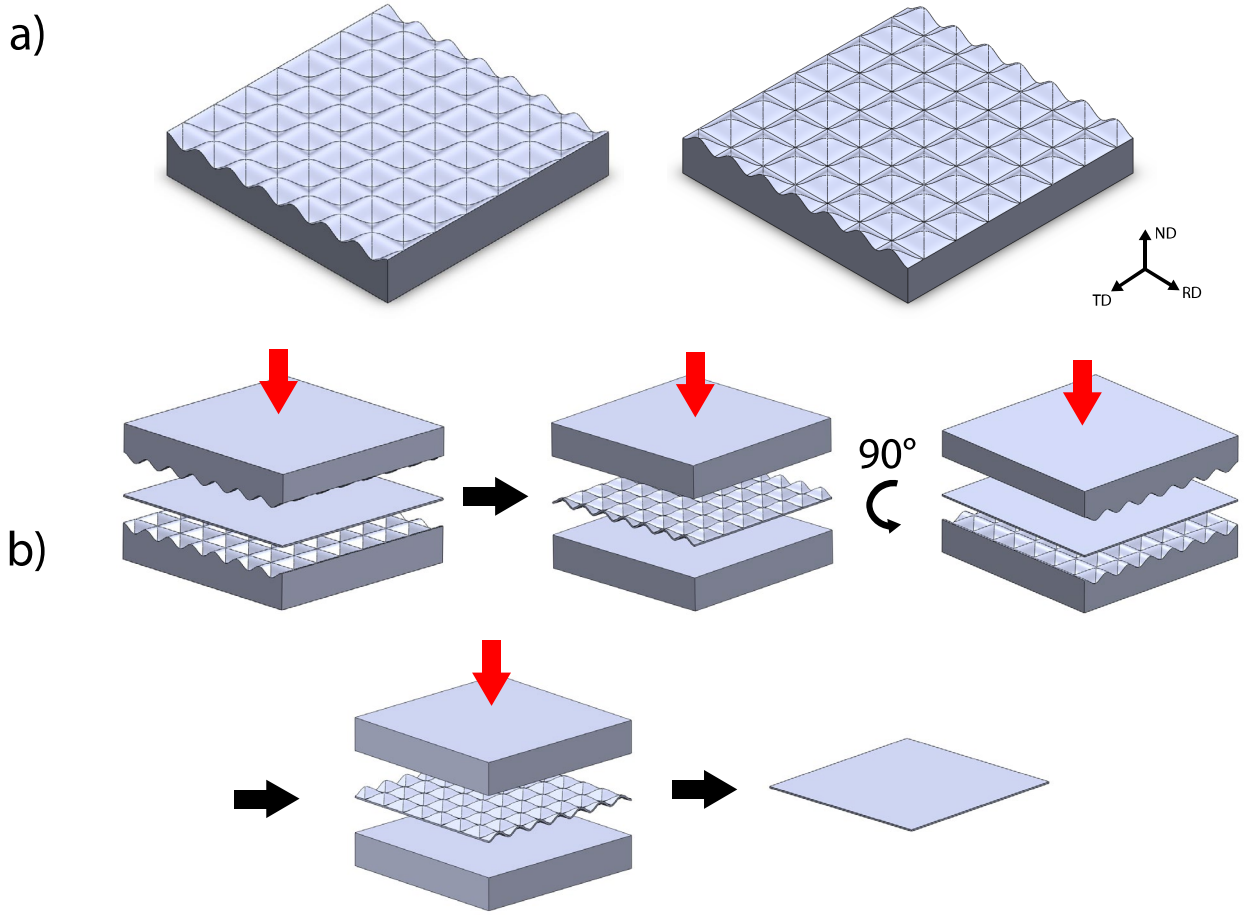

Figure 1 (a) Die profile. (b) One pass of RCS.

Materials Research Proceedings **32** (2023) 362-370 https://doi.org/10.21741/9781644902615-41

Table 1. Nominal composition of the aluminum alloys investigated in %wt [17–19].

Alloy	Si	Fe	Cu	Mn	Mg	Cr	Zn	Ti	Ni	Al
5754-H111	0.04	0.17	0.00	0.01	3.00	0.22	0.00	0.02	0.00	balance
6061-T6	0.77	0.24	0.16	0.03	1.03	0.07	0.03	0.02	0.00	balance
7075-O	0.00	0.3	1.8	0.00	2.2	0.28	5.3	0.06	0.01	balance

The hardening potential of the RCS process in the different aluminum alloys is compared based on the microhardness evolution. Therefore, Vickers microhardness measurements were taken in the deformed zone with a load of 100g ($HV_{0.1}$) with a holding time of 15 seconds. Before the hardness measurement, a representative part of a specimen was mechanically grounded and polished until mirror-finish for each composition.

Uniaxial tensile tests were conducted only for the 5754 and 6061 alloys. The tests were carried out on RCS samples subjected to one and two passes within the temperature range of 150 – 500 °C and strain rates between 3×10^{-5} and 3×10^{-2}. Figure 2 depicts the geometry of these samples, which possess a gauge length of 50 mm. Tensile tests were carried out on specimens after one and two RCS passes. These tests were performed using an INSTRON 5584 universal testing machine outfitted with a cylindrical furnace. The strain rate sensitivity coefficient (m) was derived following Equation (1).

$$\sigma = K\dot{\varepsilon}^m \tag{1}$$

where σ is the stress, K a material constant, and $\dot{\varepsilon}$ the strain rate. A pair of samples were examined for every distinct pairing of temperature and strain rate. Peak values recorded for tensile stress and associated strain rates were graphically represented on a logarithmic scale. Subsequently, a linear approximation of the data was undertaken. The slope of this plot reflects the strain rate sensitivity.

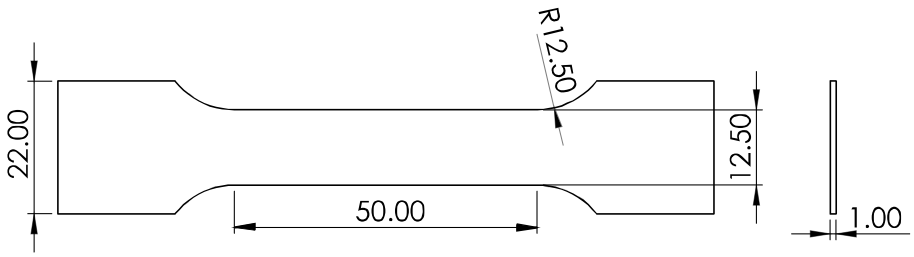

Figure 2 Dimensions of the sample employed for the hot tensile test in mm.

Finally, the crystallographic texture was determined utilizing a Rigaku Ultima IV diffractometer, operating with a Cu-Kα wavelength. The apparatus was arranged in 'in-plane' mode, with an angle range α spanning from 0.5 to 90º and β from 0 to 360º. Specimens were meticulously prepared to mirror-finish prior to the measurements. Orientation distribution functions (ODFs), typically used to represent the crystallographic orientation within Euler's space, were computed from the experimentally derived pole figures (111), (200), and (220). These ODFs were calculated using the MATLAB® toolbox MTEX software for samples in their initial condition and following one and two RCS cycles.

Materials Research Proceedings **32** (2023) 362-370 https://doi.org/10.21741/9781644902615-41

Results

Table 2 displays the average hardness values for the samples subjected to the RCS process up to two passes for the different aluminum alloys. These tests offer insight into the effects of the different hardening mechanisms on the RCS process.

Table 2. Microhardness values of the samples before and after being processed by RCS.

Average (HV0.1)	Initial condition	1P	2P
5754-H111	71.7	87.2	91.3
6061-T6	120	139.6	147.2
7075-O	66.2	76.5	75.4

The microhardness data demonstrate significant variations in hardness for different aluminum alloys subjected to the RCS process. In the case of the aluminum alloy 5754, a marked hardness increment of 22% was observed after one pass (1P), which further escalated to a 27% increase after two passes (2P). A similar trend was detected for aluminum alloy 6061-T6, albeit with slightly lower increments of 16.3% and 22% after the 1P and 2P conditions, respectively. Lastly, the hardness testing on aluminum alloy 7075-O revealed a comparable progression, registering an approximate increase of 15% in hardness for the 1P sample relative to its initial condition, and keep constant for further passes.

The most significant increase in microhardness is observed in the first RCS pass, a typical behavior typical of severe plastic deformation processes. However, in the 5754 alloy, the increase in the first pass is greater than that in the 6061 and 7075 alloys, which show a similar increase in the first pass. On the other hand, for the second RCS pass, the alloys whose primary hardening mechanism is precipitation tend to saturate more quickly. A non-significant hardness change was reported for RCS-processed alloy 7075 from the first to fourth RCS passes [19]. This result accords with the superior strain-hardening capacity of the 5754 alloy.

The increment in hardness might be attributable to the substantial dislocation density and grain boundaries induced by the RCS procedure. However, the nearly steady mechanical strength observed following the initial RCS pass could likely be ascribed to the concurrent influence of micro and ultrafine grains. The microscale grains might permit substantial deformations, thereby contributing to ductility, while the ultrafine grains could serve as barriers to the creation and sliding of dislocations, thereby enhancing the material's resistance.

Figure 3a and Figure 3b show the strain rate sensitivity coefficients at different temperatures for 6061 and 5754 samples undergoing one and two RCS cycles. It can be observed that both alloys exhibit relatively high values of the strain rate sensitivity 'm' coefficient at the tested conditions when compared with the typical values reported for aluminum alloys.

Materials Research Proceedings **32** (2023) 362-370 https://doi.org/10.21741/9781644902615-41

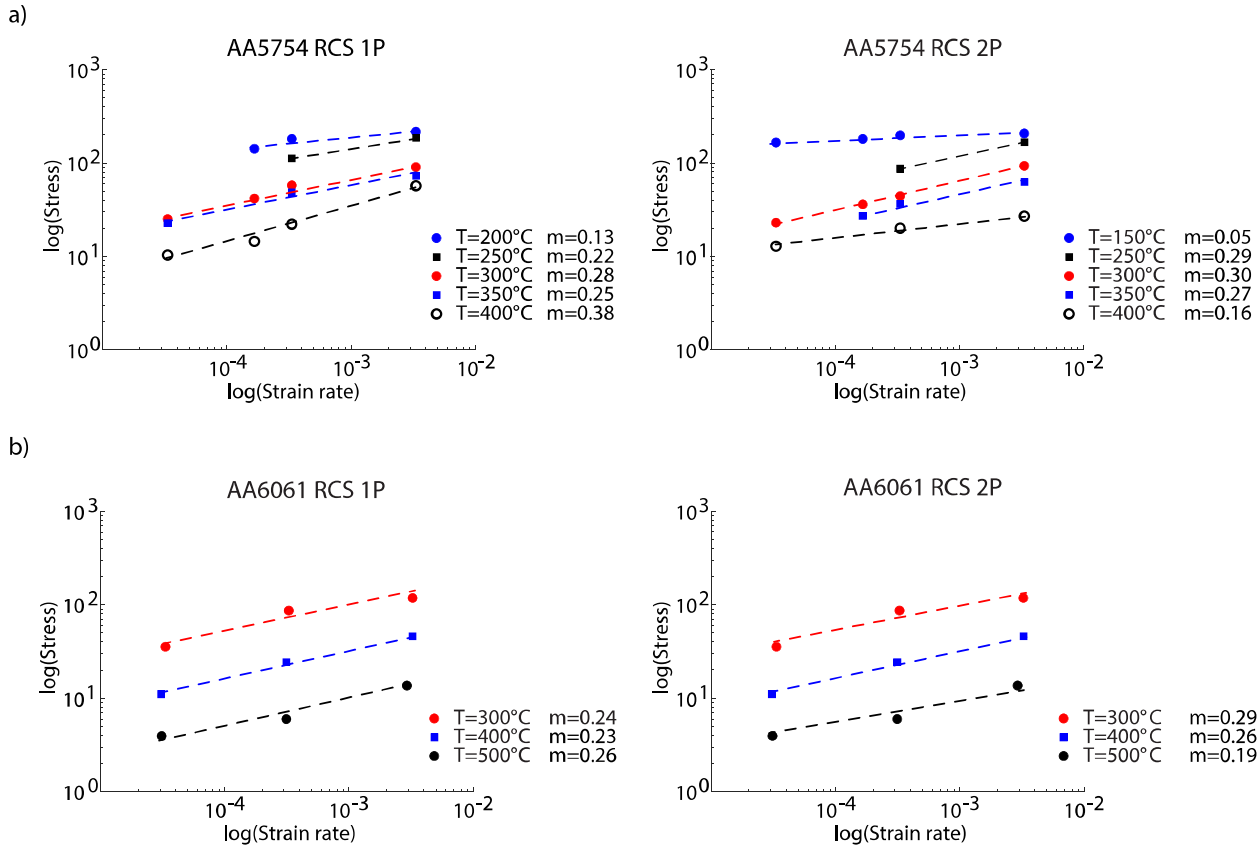

Figure 3 Strain rate sensitivity analysis of the RCS processed samples for a) AA5754 b) AA6061.

The highest 'm' value of 0.38 was achieved at 400 °C for the aluminum 5754 for one RCS pass, while the aluminum 6061 was at 300 °C for two RCS passes with a value of 0.29. Such value is similar to the exhibited by the 5754 in the same condition. On the other hand, the same trend can be observed in both alloys. For the one-pass condition, the 'm' values increase as the temperature rises, while this behavior is the opposite for two passes. They are showing the maximum value for that condition at 300 °C and getting lower as the temperature rises. The grain refinement obtained after the RCS processed samples could explain the high values for the strain rate sensitivity coefficients, since the grain size plays an important role in the deformation mechanisms at these temperatures. Furthermore, the inverse behavior in the two RCS passes could be because the recrystallization temperature decreased due to the deformation process, impacting the activation temperature associated with the deformation mechanism. This results in an enhanced capacity of uniform deformation at high temperatures given by the RCS process.

The quantitative analysis of the volume fraction of the different texture components that are typically developed in aluminum alloys was calculated from the ODF. Table 3 shows the result for the different alloys. Firstly, the aluminum alloy 5754-H111 exhibits a predominantly mixed texture, primarily composed of β-fiber and S-Cube fiber components. The β-fiber texture is defined by a series of <111> fiber textures that spread in the φ_2=45° section of an orientation distribution function (ODF). This texture component is typically observed in metals undergoing processes like rolling or drawing. On the other hand, a connecting fiber, S-Cube fiber, has been previously identified as a potential pathway for recrystallization leading to Cube. These observed texture components align well with the material's thermomechanical history, which underwent a process of rolling, leading to the generation of the S component, followed by an annealing process, resulting in the production of the S-Cube fiber. Throughout the process, the texture components remain consistent. However, there is a minor decrease in the intensity correlating with the number

of RCS passes. This reduction in β-fiber, along with the lack of additional β-fiber generation during the process, could positively impact the material's forming capacity, given that previous studies suggest that the presence of β-fiber can be detrimental to the material's formability.

In the case of the aluminum alloy 6061-T6, the initial condition prominently exhibits a strong cube texture, characteristic of the annealed texture commonly found in aluminum alloys. This texture aligns well with the material's thermomechanical history because of the solid solution treatment performed previous to the aging needed to reach the T6 condition. As the number of RCS passes increases, the S component significantly increases. In addition, when subjected to two RCS cycles, a non-common texture component appears. This emergent texture component might be associated with the bending process inherent to the RCS process. Moreover, a substantial reduction in the intensity of the Cube texture component is evident. Literature suggests that this decrease in intensity relates to the rotation of some texture components induced by the bending state [20].

In the initial state of the 7075-O alloy, a prominent Cube orientation is discernible, likely attributable to the recrystallized grains formed during the annealing process. This texture aligns with the findings observed in the 6061 alloys. Interestingly, the Goss and P orientations also manifest in approximately equal measures. A significant observation is that as the intensity of the Cube texture dwindles, other texture components essentially sustain their presence. This pattern is evident across all three studied alloys, where the dominant texture component significantly decreases in intensity with each additional RCS pass. The marked decrease in Cube texture intensity concurrent with increasing applied deformation is consistent with numerous studies on rolled Al-based alloys.

Table 3. Quantitative analysis of the texture evolution through the RCS process.

Texture component	5754			6061			7075		
	0P	1P	2P	0P	1P	2P	0P	1P	4P
Goss	2.3	2.0	1.7	-	-	-	14.0	18.9	14.5
P	-	-	-	-	-	-	13.9	14.4	10.6
Brass	6.6	5.1	3.9	-	1.4	3.8	-	-	-
S	25.9	21.7	21.7	3.1	7.1	12.2	-	-	-
Cu	6.3	5.7	6.0	-	-	-	-	-	-
Cube	-	-	-	46.9	44.1	17.8	13.7	5.3	2.8
S-Cube connecting fiber	18.3	18.3	17.9	9.5	9.9	5.3	-	-	-

Conclusions

In conclusion, the Repetitive Corrugation and Straightening (RCS) process was applied to commercially available 5754, 6061, and 7075 aluminum alloys. The results displayed a significant hardening effect in the alloys, with distinct hardening mechanisms influencing the process. Microhardness tests revealed a significant increase in hardness, particularly for the 5754 alloy, which showed the greatest hardening potential. The rise in hardness is likely attributable to the high dislocation density and grain boundaries introduced by the RCS process.

Tensile tests conducted at different temperatures and strain rates showed 6061 and 5754 alloys exhibiting relatively high strain rate sensitivity 'm' coefficients. A peak 'm' value appears at specific temperatures for one and two RCS passes, providing further evidence of grain refinement's impact on the deformation mechanisms and the alloy's mechanical properties.

Crystallographic texture analysis showed that the RCS process had distinct effects on different alloy textures. In particular, the process significantly reduced the cube texture component in all the studied alloys, with the effect being most pronounced in the 7075-O alloy. The consistency in

the other texture components suggests that the Goss and S texture components are able to remain during the RCS process.

In summary, the RCS process presents an effective approach to enhance the mechanical properties of the studied aluminum alloys. This study provides insight into the potential of the RCS process for industrial applications, such as automotive and aerospace, where enhanced mechanical properties are of significant importance. However, more comprehensive investigations considering more complex deformation processes and additional alloy types may be necessary to understand the RCS's potential better.

References

[1] Z. Chen, G. Fang, J.-Q. Zhao, Formability Evaluation of Aluminum Alloy 6061-T6 Sheet at Room and Elevated Temperatures, J. of Materi Eng and Perform. 26 (2017) 4626–4637. https://doi.org/10.1007/s11665-017-2895-0.

[2] W.S. Miller, L. Zhuang, J. Bottema, A.J. Wittebrood, P. De Smet, A. Haszler, A. Vieregge, Recent development in aluminium alloys for the automotive industry, Materials Science and Engineering: A. 280 (2000) 37–49. https://doi.org/10.1016/S0921-5093(99)00653-X.

[3] R.Z. Valiev, R.K. Islamgaliev, I.V. Alexandrov, Bulk nanostructured materials from severe plastic deformation, Progress in Materials Science. 45 (2000) 103–189. https://doi.org/10.1016/S0079-6425(99)00007-9.

[4] H. Yu, L. Su, C. Lu, K. Tieu, H. Li, J. Li, A. Godbole, C. Kong, Enhanced mechanical properties of ARB-processed aluminum alloy 6061 sheets by subsequent asymmetric cryorolling and ageing, Materials Science and Engineering: A. 674 (2016) 256–261. https://doi.org/10.1016/j.msea.2016.08.003.

[5] J. Huang, Y.T. Zhu, D.J. Alexander, X. Liao, T.C. Lowe, R.J. Asaro, Development of repetitive corrugation and straightening, Materials Science and Engineering: A. 371 (2004) 35–39. https://doi.org/10.1016/S0921-5093(03)00114-X.

[6] D.H. Shin, J.-J. Park, Y.-S. Kim, K.-T. Park, Constrained groove pressing and its application to grain refinement of aluminum, Materials Science and Engineering: A. 328 (2002) 98–103. https://doi.org/10.1016/S0921-5093(01)01665-3

[7] L. Romero-Resendiz, J.M. Cabrera, S. Elizalde, V. Amigó-Borrás, I.A. Figueroa, G. Gonzalez, Mechanical, stress corrosion cracking and crystallographic study on flat components processed by two combined severe plastic deformation techniques, Journal of Materials Research and Technology. 18 (2022) 1281–1294. https://doi.org/10.1016/j.jmrt.2022.03.010

[8] M. Ezequiel, I.A. Figueroa, S. Elizalde, J.M. Cabrera, C. Braham, L. Morin, G. Gonzalez, Numerical and experimental study of a 5754-aluminum alloy processed by heterogeneous repetitive corrugation and straightening, Journal of Materials Research and Technology. 9 (2020) 1941–1947. https://doi.org/10.1016/j.jmrt.2019.12.026

[9] A. Azushima, R. Kopp, A. Korhonen, D.Y. Yang, F. Micari, G.D. Lahoti, P. Groche, J. Yanagimoto, N. Tsuji, A. Rosochowski, A. Yanagida, Severe plastic deformation (SPD) processes for metals, CIRP Annals. 57 (2008) 716–735. https://doi.org/10.1016/j.cirp.2008.09.005.

[10] E. Bruder, Formability of Ultrafine Grained Metals Produced by Severe Plastic Deformation-An Overview, Adv. Eng. Mater. 21 (2019) 1800316. https://doi.org/10.1002/adem.201800316.

[11] A.A. Khamei, K. Dehghani, Effects of strain rate and temperature on hot tensile deformation of severe plastic deformed 6061 aluminum alloy, Materials Science and Engineering: A. 627 (2015) 1–9. https://doi.org/10.1016/j.msea.2014.12.081

[12] S. Suwas, R.K. Ray, Crystallographic Texture of Materials, Springer London, London, 2014. https://doi.org/10.1007/978-1-4471-6314-5

[13] J. Galán-López, L.A.I. Kestens, Optimization of Crystallographic Texture for Sheet-forming Applications Using Taylor-based Models, Metall Mater Trans A. 49 (2018) 5745–5762. https://doi.org/10.1007/s11661-018-4869-8

[14] K. Yoshida, T. Ishizaka, M. Kuroda, S. Ikawa, The effects of texture on formability of aluminum alloy sheets, Acta Materialia. 55 (2007) 4499–4506. https://doi.org/10.1016/j.actamat.2007.04.014

[15] F. Barlat, O. Richmond, Prediction of tricomponent plane stress yield surfaces and associated flow and failure behavior of strongly textured f.c.c. polycrystalline sheets, Materials Science and Engineering. 95 (1987) 15–29. https://doi.org/10.1016/0025-5416(87)90494-0

[16] K. Ma, H. Wen, T. Hu, T.D. Topping, D. Isheim, D.N. Seidman, E.J. Lavernia, J.M. Schoenung, Mechanical behavior and strengthening mechanisms in ultrafine grain precipitation-strengthened aluminum alloy, Acta Materialia. 62 (2014) 141–155. https://doi.org/10.1016/j.actamat.2013.09.042

[17] S. Elizalde, M. Ezequiel, I.A. Figueroa, J.M. Cabrera, C. Braham, G. Gonzalez, Microstructural Evolution and Mechanical Behavior of an Al-6061 Alloy Processed by Repetitive Corrugation and Straightening, Metals. 10 (2020) 489. https://doi.org/10.3390/met10040489

[18] M. Ezequiel, S. Elizalde, J.-M. Cabrera, J. Picas, I.A. Figueroa, I. Alfonso, G. Gonzalez, Formability of the 5754-Aluminum Alloy Deformed by a Modified Repetitive Corrugation and Straightening Process, Materials. 13 (2020) 633. https://doi.org/10.3390/ma13030633

[19] L. Romero-Resendiz, V. Amigó-Borrás, A. Vicente-Escuder, S. Elizalde, J.M. Cabrera, D. Pineda-Ruiz, I.A. Figueroa, G. Gonzalez, Effect of the microstructure generated by Repetitive Corrugation and Straightening (RCS) process on the mechanical properties and stress corrosion cracking of Al-7075 alloy, Journal of Materials Research and Technology. 15 (2021) 4564–4572. https://doi.org/10.1016/j.jmrt.2021.10.043

[20] W. Muhammad, U. Ali, A.P. Brahme, J. Kang, R.K. Mishra, K. Inal, Experimental analyses and numerical modeling of texture evolution and the development of surface roughness during bending of an extruded aluminum alloy using a multiscale modeling framework, International Journal of Plasticity. 117 (2019) 93–121. https://doi.org/10.1016/j.ijplas.2017.09.013